

Quantitative characterization of endoscopic imaging fibers

HARRY A. C. WOOD,^{*} KERRIANNE HARRINGTON, JAMES M. STONE, TIM A. BIRKS, AND JONATHAN C. KNIGHT

Centre for Photonics and Photonic Materials, Department of Physics, University of Bath, Bath, BA27AY, UK

[*h.wood@bath.ac.uk](mailto:h.wood@bath.ac.uk)

Abstract: We describe a technique for the quantitative characterization of endoscopic imaging fibers using an interference pattern as the standard object to be imaged. The visibility of the pattern at the other end of the fiber is then analyzed as wavelength and fringe period are varied. We demonstrate the use of the technique by comparing three fibers: two fabricated in-house from the same preform, designed to minimize inter-core coupling at visible wavelengths less than 650 nm, and a commercial imaging fiber. The techniques discussed are currently being used to optimize fibers for fluorescence bronchoscopy to be used in intensive care clinics.

Published by The Optical Society under the terms of the [Creative Commons Attribution 4.0 License](#). Further distribution of this work must maintain attribution to the author(s) and the published article's title, journal citation, and DOI.

OCIS codes: (060.2270) Fiber characterization; (060.2350) Fiber optics imaging; (170.0170) Medical optics and biotechnology; (170.3880) Medical and biological imaging; (170.3890) Medical optics instrumentation.

References and links

1. C. M. Lee, C. J. Engelbrecht, T. D. Soper, F. Helmchen, and E. J. Seibel, "Scanning fiber endoscopy with highly flexible, 1 mm catheterscopes for wide-field, full-color imaging," *J. Biophotonics* **3**(5-6), 385–407 (2010).
2. X. Chen, K. L. Reichenbach, and C. Xu, "Experimental and theoretical analysis of core-to-core coupling on fiber bundle imaging," *Opt. Express* **16**(26), 21598–21607 (2008).
3. A. W. Snyder and J. D. Love, *Optical Waveguide Theory* (Chapman and Hall, 1983).
4. M. Koshiba, K. Saitoh, and Y. Kokubun, "Heterogeneous multi-core fibers: proposal and design principle," *IEICE Electron. Express* **6**(2), 98–103 (2009).
5. K. Saitoh, M. Koshiba, K. Takenaga, and S. Matsuo, "Homogeneous and Heterogeneous Multi-core Fibers," *Opt. Express* **20**(2), 949–959 (2012).
6. N. Ortega-Quijano, F. Fanjul-Vélez, and J. L. Arce-Diego, "Optical crosstalk influence in fiber imaging endoscopes design," *Opt. Commun.* **283**(4), 633–638 (2010).
7. B. Zhang, C. Zhai, S. Qi, W. Guo, Z. Yang, A. Yang, X. Gai, Y. Yu, R. Wang, D. Tang, G. Tao, and B. Luther-Davies, "High-resolution chalcogenide fiber bundles for infrared imaging," *Opt. Lett.* **40**(19), 4384–4387 (2015).
8. P. Russell, "Photonic Crystal Fibers," *Science* **299**(5605), 358–362 (2003).
9. T. Butz, *Fourier Transformation for Pedestrians* (Springer, 2006).
10. J. H. Chang, H. G. Choi, S. H. Bae, D. H. Sim, H. Kim, and Y. C. Chung, "Crosstalk analysis in homogeneous multi-core two-mode fiber under bent condition," *Opt. Express* **23**(8), 9649–9657 (2015).
11. "Data for Quantitative characterization of endoscopic imaging fibers," <https://doi.org/10.15125/BATH-00325>

1. Introduction

Endoscope technology has remained largely unchanged since the 1950s despite advances across other fields of optics. It has been shown that while using some of the most common endoscopic instruments the clinicians' vision is reduced to that of someone who would be legally considered blind [1]. Recent developments in telecoms technology represent an opportunity to improve the design and fabrication techniques of the coherent fiber bundles used for endoscopy, which should lead to swift development of this field over the coming years.

We demonstrate a technique capable of characterizing the performance of coherent fiber bundles as a function of wavelength, using one commercial and two in-house imaging fibers. This technique enables the characterization of new endoscopic imaging fibers to optimize

their performance for the specific procedures. Our specific interest is in providing improved resolution at wavelengths relevant for fluorescence imaging.

The spatial resolution of images obtainable using a coherent fiber bundle is the result of balancing the number of pixels (the number of cores per unit area of the field of view) with blurring of the image due to the inter-core coupling (crosstalk) which inevitably arises when cores are packed too close together [2, 3]. The deterioration of imaging quality with increasing wavelength due to increased coupling as the mode fields from adjacent cores spread, overlap, and exchange energy, which usually results in an effective upper wavelength limit [2]. One technique to reduce inter-core coupling that is commonly employed in multicore telecoms fibers involves arranging the cores so that the guided modes in no two neighboring cores have the same modal index [4]. This has allowed better space division multiplexing as more cores can be packed within the same diameter fiber without information being lost to core crosstalk [4, 5]. It has been shown that these methods can be adapted to improve the optical performance of imaging fibers by varying the size of neighboring cores [6]; a technique that we have employed in a multi-stage stack and draw process to produce some of the fibers used during the course of this work.

During the iterative process of design and fabrication used to produce the fibers investigated in the course of this research it was essential to be able to quantitatively compare fibers with one another, as well as with commercially available equivalents, to determine whether design changes lead to improved imaging quality. For this purpose many groups use imaging standards such as US Air Force test targets to qualitatively compare their fibers [2, 7]. We have found that while these methods are sufficient to highlight large differences in the fibers' operating wavelengths and resolutions, an accurate and quantitative comparison is needed in order to characterize the more subtle differences that occur between fibers designed to operate within similar regimes.

One method to explore the effects of crosstalk on imaging quality is to couple light of various wavelengths into a single core and observe the spread to other cores [2]. However, a significant fraction of the cores should be tested using this method if an accurate comparison of fibers is to be obtained; an unrealistic task for fibers with tens of thousands of cores.

Instead, we quantitatively analyses the imaging quality of the entire field of view using an interference pattern of variable period and wavelength as the standard image. The transmitted images are then scrutinized using two separate methods.

2. Method

Figure 1 depicts the characterization setup we used to investigate the fibers. The supercontinuum (1) source is coupled into an Edmund Optics mini-monochromator (#53-954) (2) to provide a tunable wavelength source. By using a beam splitter and a delay arm (3) the beams can be interfered on the test fiber's (4) input end. This interference pattern is used as the test object, the wavelength-dependent period of which is variable by changing the angle θ between the beams. Achromatic lenses were used after the monochromator, allowing the wavelength to be scanned easily without it being necessary to refocus. The camera (5) was used to take the output images from the test fiber for analysis. For consistency of illumination we ensured that the fiber's input face is as close as possible to perpendicular to the bisector of the angle of recombination of the two interfering beams, by observing that the reflection of one beam from the test fiber's end face aligns with the other beam.

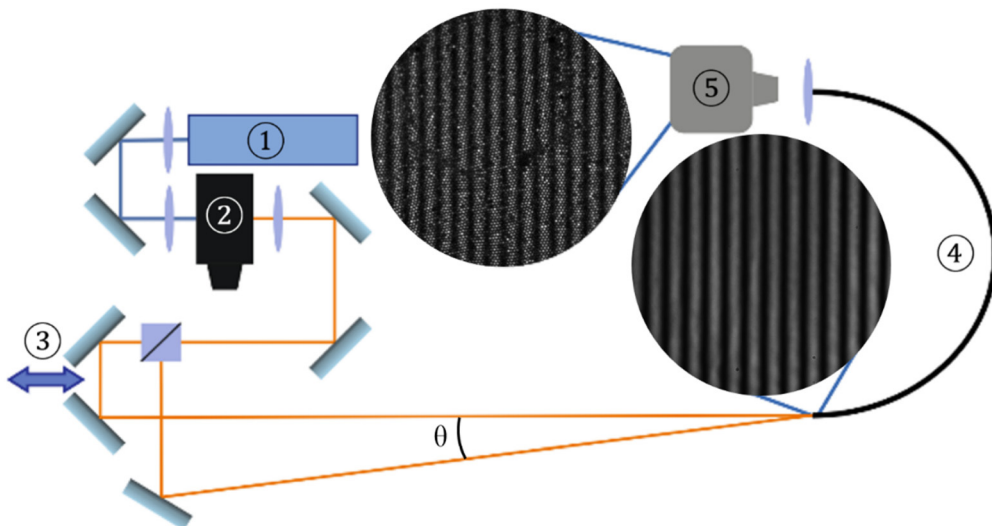


Fig. 1. Diagram of the apparatus used: (1) supercontinuum source, (2) mini-monochromator (3) delay line mirrors (4) imaging fiber under test (5) camera. The insets show an image of the interference pattern formed on the input end of the fiber and the resulting near field image at the test fiber's output.

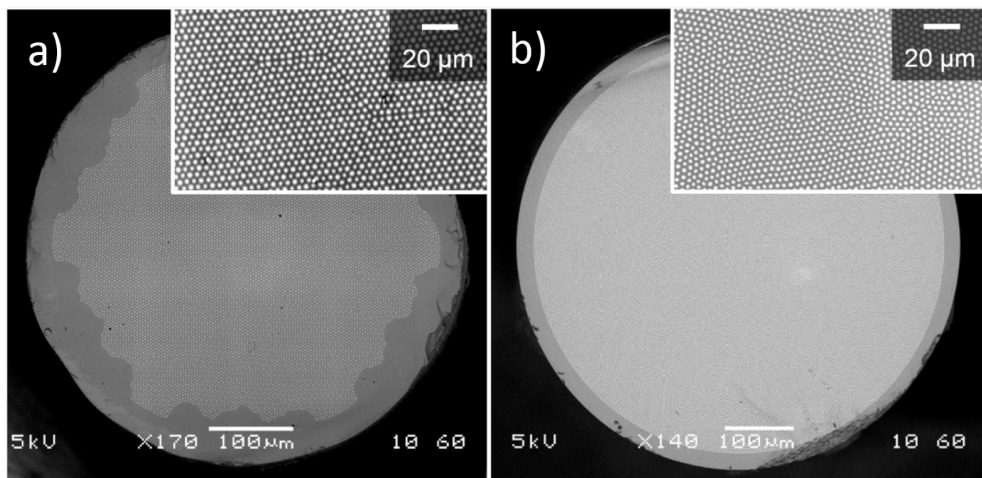


Fig. 2. SEM images of the end face of fibers (a) B1 and (b) FIGH-30-650s, with insets showing magnified images of the fibers' core patterns.

Three imaging fibers have been investigated using this technique; two were fabricated in-house and the third was Fujikura's FIGH-30-650s. The fibers B1 and B2 fabricated in house were drawn from the same preform and so have identical structures but different scales, with outer diameters of 525 μm and 470 μm respectively. An SEM image of B1 is shown in Fig. 2(a). The structure of B1 and B2 was designed to minimize core crosstalk at visible wavelengths below 650 nm.

The preform from which they were drawn was made in three stages using stack and draw techniques commonly used in the fabrication of photonic crystal fibers [8]. In the first stage, nominally-identical germanium-doped graded index preforms of numerical aperture NA = 0.3 were purchased from Draka-Prysmian (OM1 PCVD rod) and drawn down to 16 canes of 5 mm diameter and 111 canes of 1 mm diameter. The 5 mm canes were jacketed using pure silica tubes, half of 6.57 mm outer diameter and the rest of 5.67 mm outer diameter. These

were drawn down to produce two sets of 110 canes of 1 mm diameter. The outcome of this procedure was three sets of canes with the same outer diameter of 1 mm but different core diameters.

In the second stage these canes were arranged into a closed-packed hexagonal stack of 331 canes so that no two canes with the same core size neighbored each other. This stack was drawn down to 37 canes of 2.1 mm flat-to-flat width.

In the third stage, the 37 canes were in turn assembled into a hexagonal stack. This stack was inserted into a jacketing tube of 10.9 mm inner and 12 mm outer diameter, and the gaps between the stack and tube were packed with pure silica canes to yield a 12247 core preform. This was drawn under partial vacuum to collapse all remaining air gaps and produce the two final fibers.

Having two fibers of identical structure but different sizes is useful as they are expected to function identically but at different wavelengths; at a fixed wavelength the smaller of the two should experience increased core to core coupling effects. The SEM image in Fig. 2(b) is FIGH-30-650s, the commercial fiber used for comparison in this work. All three fibers were polished at both ends in preparation for characterization.

The images of the fringes, captured by the camera at the output of each fiber, were analyzed in two ways: First, the columns of pixels were vertically averaged, to produce a binned intensity distribution as a function of the horizontal pixel coordinate x , Fig. 3. This distribution was fitted to a curve in the form of Eq. (1):

$$I(x) = a_0 + a_1 \sin^2(bx + c) \quad (1)$$

The visibility of the fringes can be calculated using

$$\text{visibility} = \frac{a_1}{a_1 + a_0} \quad (2)$$

By mounting the camera on a goniometer the camera's CCD was accurately aligned to the fringe pattern from the end of the fiber despite any twists along the fiber's length.

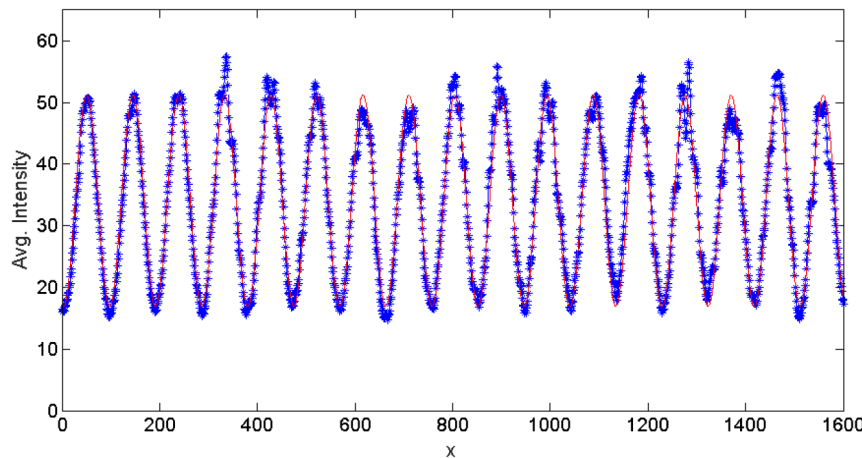


Fig. 3. A typical binned intensity distribution (blue points) with the fit to Eq. (1) (red curve).

The second method involves taking the Fourier transform of the images, Fig. 4. The three peaks near the middle of the transformed image, at relatively low spatial frequencies, represent the image's "d.c." brightness flanked by two peaks from the sinusoidal variation of the fringe pattern. In order to sharpen these side peaks we multiplied the original image data by a Gaussian window [9] before taking the 2-D FFT. The combined intensity of the side peaks was normalized by that of the central peak to provide a measure of the fidelity of the

transmitted interference pattern. We call this the Fourier contrast and note that, unlike the binning method, it is insensitive to misalignment of the fringe pattern to the axes of the camera sensor.

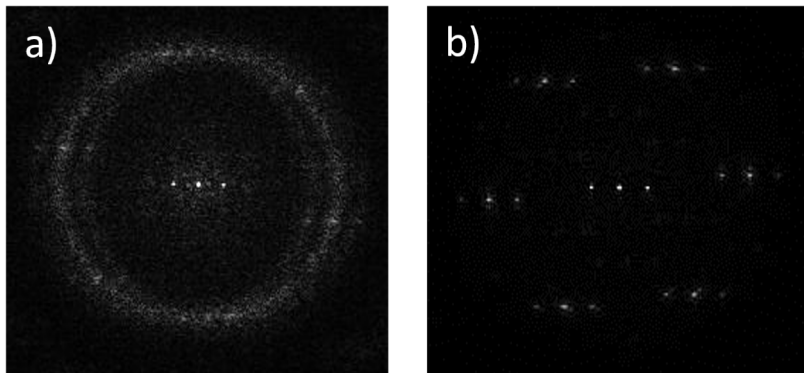


Fig. 4. Calculated Fourier transforms of typical interference pattern viewed via (a) FIGH-30-650s and (b) B1.

The Fourier transforms were also useful for highlighting differences in the structures of the fibers. The higher spatial-frequency features around the three central peaks are the transforms of the core pattern. Due to the lack of long range order in the core pattern of the FIGH-30-650s, this manifests as a circular ring, copied 3 times due to convolution with the 3 central peaks, as can be seen in Fig. 4(a). In contrast, the regular hexagonal lattice of B1 produces a clearly-defined set of 6 peaks, again copied 3 times, in Fig. 4(b).

3. Results

Figure 5 shows fringe visibility data obtained by the binning (a) and Fourier (b) methods analyzing the same set of images that were acquired using each of the 3 fibers across a range of wavelengths from 500 to 700 nm. The beam angle of $\theta = 2.29^\circ$ was chosen so that the fringe period was $15 \mu\text{m}$ for wavelength $\lambda = 600 \text{ nm}$; fringe period will of course scale in proportion to λ . The two plots show the same trends for each of the fibers, and the crossing points of each curve occur at similar wavelengths for the two analysis techniques, confirming that the more versatile Fourier method captures the same behavior as the more readily understood binning method. The close correlation between the binning-derived visibility and the Fourier contrast is shown by the inset to Fig. 5(a).

The slightly more closely-packed cores of B1 and B2 give them better imaging resolution at shorter wavelengths than FIGH-30-650s. The performance of B1 and B2 then falls off rapidly towards the longer wavelengths, as their smaller and closer cores are more susceptible to coupling. This effect is also illustrated by the comparison between B1 and B2. Both fibers were drawn from the same preform and so have the same number of cores, core-cladding index contrast and core size-to-spacing ratio. Since B2 was drawn to a smaller scale than B1, its performance curve is similar to that of B1 but shifted towards shorter wavelengths. The upward trend for FIGH-30-650s was unexpected, but can be explained by a flat performance profile combined with the increase in fringe period with wavelength, as expected for an interference pattern.

Figure 6 shows portions of some of the fringe images used to produce Fig. 5. Of particular note are the higher-order modes visible where the cores are supposed to be dark. These are presumably excited through inter-core crosstalk, and are most apparent in Fig. 6(c). The differences in the structure of the coupled light are also interesting: In FIGH-30-650s crosstalk manifests as “tendrils” of light crossing the dark fringes due to the groups of

similarly sized neighboring cores; however in B1 the regular structure leads to a more uniform loss of visibility.

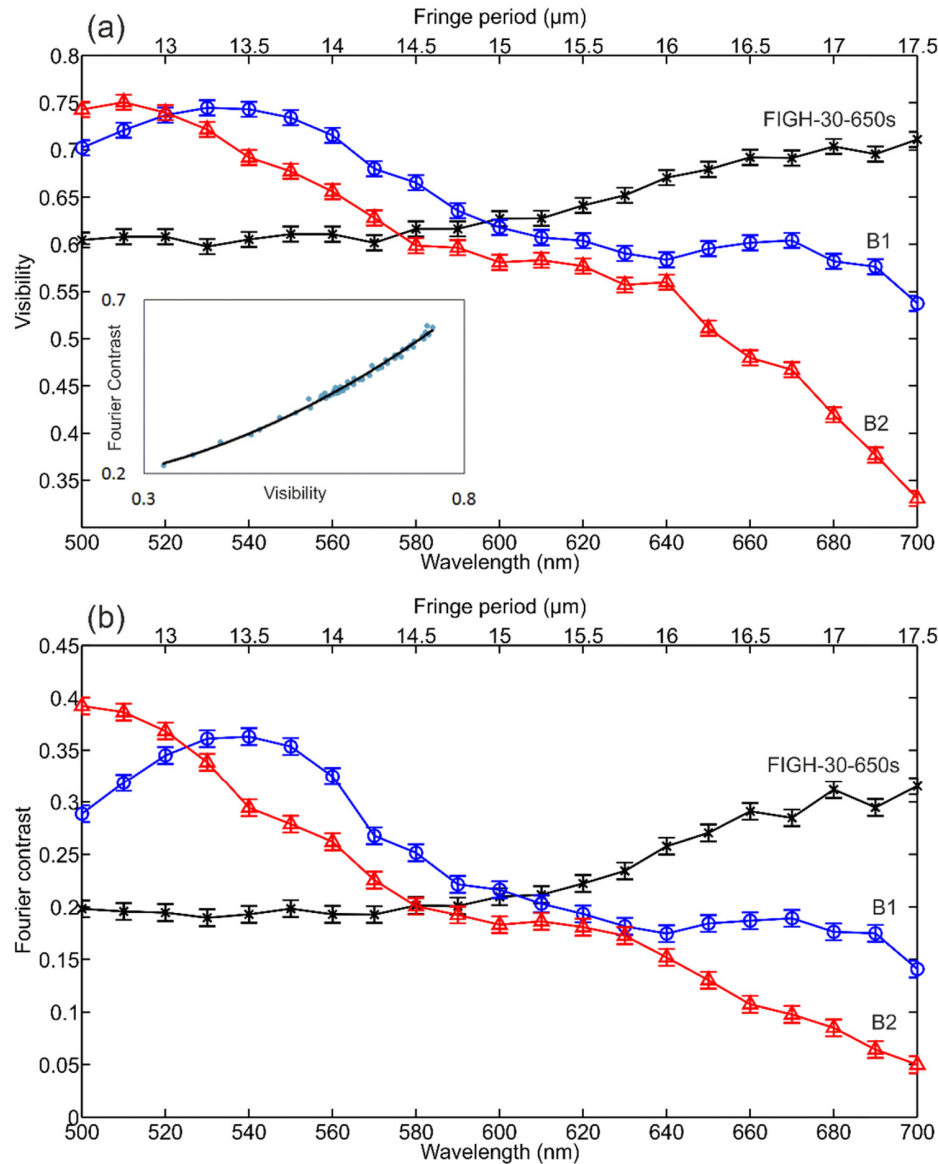


Fig. 5. Fringe visibility determined by binning method (a) and Fourier method (b) for each of the three fibers, versus wavelength. Error bars represent the standard deviation of a series of data points taken at a single wavelength, realigning the system between each measurement. The beam angle θ of 2.29° was chosen to give a fringe period of $15 \mu\text{m}$ at $\lambda = 600 \text{ nm}$; the period at other wavelengths is indicated on the upper x axis. The inset in (a) is a plot of each wavelength's Fourier contrast value (y-axis) against its corresponding binning-derived visibility value (x-axis), with a quadratic fit $y = 0.9416x^2 - 0.1051x + 0.1616$.

For comparison, Fig. 7 shows four images of US Air Force test targets obtained using FIGH-30-650s and B1. In each case the test target was placed in contact with the output end of the fiber and illuminated by supercontinuum light source. The output was filtered using a bandpass filter and imaged onto a camera. B1 shows better contrast than FIGH-30-650s at

550 nm, but increased coupling means that at 650 nm the opposite is true. This is consistent with the data depicted in Figs. 5 and 6.

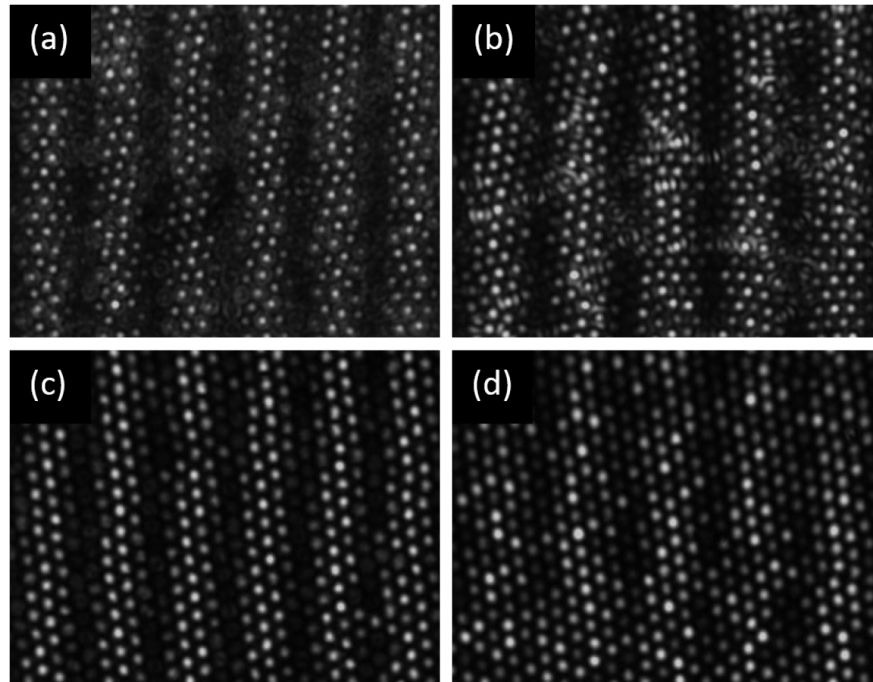


Fig. 6. Portions of cropped fringe images used to produce the data in Figs. 5 and 6. (a) & (b) were taken using FIGH-30-650s, (c) & (d) using B1. (a) & (c) used 550 nm light, (b) & (d) used 650 nm light. Each image is 80 μm across.

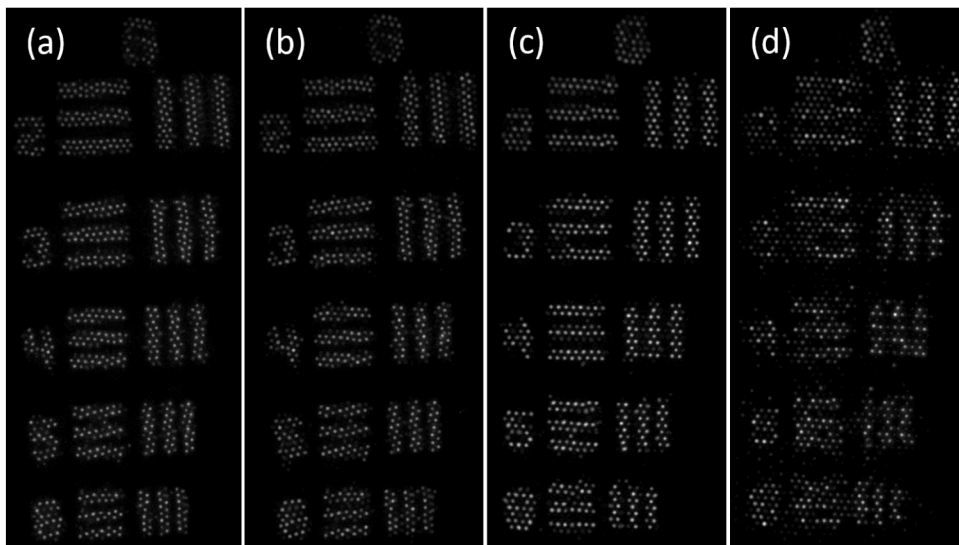


Fig. 7. Images of “group 6” elements of a US Air Force test target taken using the FIGH-30-650s (a) & (b) and B1 (c) & (d) at zero working distance, illuminated in transmission by 550 nm (a) & (c) and 650 nm (b) & (d) light. The lines of element 2 have a width of 7.81 μm .

Additional data were taken for smaller fringe spacings by increasing the beam angle to $\theta = 2.75^\circ$ so that the fringe period was 12.5 μm for $\lambda = 600 \text{ nm}$. The Fourier contrast data are

shown in Fig. 8, without the corresponding binning-derived visibility data which again followed a very similar pattern. The results are all shifted to lower contrast values compared to Fig. 5(b), as expected when imaging a finer pattern. However, the wavelength ranges where each fiber performs better are strikingly consistent between the two fringe spacings.

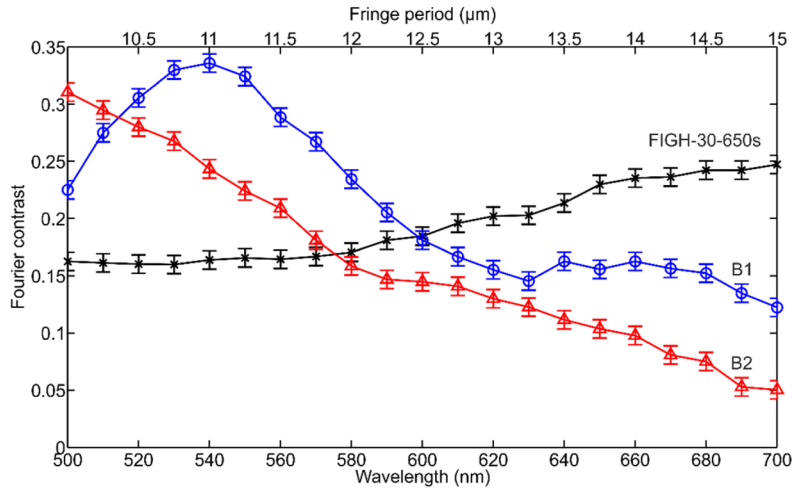


Fig. 8. Fourier contrast data corresponding to that in Fig. 5(b) but obtained using a beam angle of $\theta = 2.75^\circ$, giving a fringe period of $12.5 \mu\text{m}$ at $\lambda = 600 \text{ nm}$.

4. Conclusion

We have developed a quantitative technique to analyses the visibility of the images transmitted by coherent fiber bundles across the visible spectrum. The technique has been tested using three fibers, two of which were drawn from the same preform in-house. The results obtained were corroborated by images using US Air Force test targets, indicating that this technique can be a valuable tool in characterizing images transmitted by coherent fiber bundles.

It is notable that the imaging performance of fiber B1 is comparable to that of the commercial fiber FIGH-30-650S at green wavelengths, despite the use of core material with a lower refractive index contrast ($\text{NA} = 0.3$ rather than $\text{NA} = 0.39$ [2]).

For simplicity this paper only considers low NA illumination that preferentially excites the fundamental LP_{01} modes of the fiber cores, even though the cores support more than one mode. However, higher-order modes couple more strongly between cores [10], and we have seen image quality degraded when a USAF test target is illuminated at higher NA. Nonetheless the technique described can be easily adapted to assess this effect by tilting the input fiber end to controllably couple more light into higher order modes. Research into the effects of higher NA illumination using this technique is ongoing.

The data gathered during the course of this work are available at [11].

Funding

UK Engineering and Physical Sciences Research Council (EPSRC) (EP/K03197X/1).

Acknowledgments

We gratefully acknowledge discussions with and support from other members of the Proteus IRC at Edinburgh and Heriot Watt Universities.